AIAA JOURNAL
Vol. 41, No. 11, November 2003

Analysis of the Effects of Thin Sealant Layers in Aircraft Structural Joints

Charoenyut Dechwayukul*
Prince of Songkhla University, Hatyai, Songkhla 90112, Thailand
and
Carol A. Rubin† and George T. Hahn‡
Vanderbilt University, Nashville, Tennessee 37235-1592

A general method is devised for determining the effects of thin layers of sealants or adhesives on the mechanical behavior of riveted lap joints using finite element analysis. The resulting method, thin adhesive layer analysis (TALA), models the sealant layer with normal and shear spring elements. The TALA method is validated by comparison with existing solutions for both linear high-modulus, and nonlinear low-modulus, adhesives. It is then used to model sealants for aircraft-riveted lap joints. The analyses reveal that sealant layers introduce large increases in the in- and out-of-plane displacements, reduce bending and stress concentration factors (SCF), and increase the fatigue life of riveted lap joints.

Introduction

IN recent years adhesives have been widely used to bond metallic-to-metallic and metallic-to-composite structural members in many engineering applications. Particularly in aircraft structures, several kinds of adhesives, for example, high modulus or structural adhesives, such as epoxy, have been used for joining structural members and minimizing sources of stress concentrations. These also provide high strength-to-weight ratios. In addition to high-modulus adhesives, low-modulus or rubber-like sealants, such as elastomers, have also been used to prevent moisture and corrosion in the riveted lap joint of aircraft fuselage structures. A thin layer of polymeric sealant, inserted between contacting surfaces, might also support a portion of the cyclic load and enhance the fatigue strength of riveted lap joints. However, the mechanical benefits of sealant combined with rivets are ill defined and poorly understood. This paper presents and validates a novel thin adhesive layer analysis (TALA) for evaluating the mechanical effects of sealants in riveted lap joints.

The analysis employs spring elements existing in the finite element commercial code ABAQUS. These spring elements are designed to reproduce the behavior of a thin layer of sealant or adhesive in the normal and shear directions. The spring elements take the place of the polymer sealant in two-dimensional and three-dimensional finite element models. The sealant-coating polymer, PRC-DeSoto PR-1776 B-2 Model 654, is used as an adhesive. Two-dimensional finite element models of adhesive and adhesive-stepped lap joints (unriveted lap joints) are compared with analytical solutions and experiments (using PR-1776) to validate TALA. TALA is then used to evaluate the effect of the sealant on the mechanical behavior of riveted lap joints. Results for sealed riveted lap joints, including compliance, rivet tilt, stress distributions, and stress concentration factors (SCF), are compared with results for unsealed riveted lap joints.

Received 27 May 2002; revision received 5 May 2003; accepted for publication 12 May 2003.

*Lecturer, Department of Mechanical Engineering, Faculty of Engineering.
†Professor, Department of Mechanical Engineering, School of Engineering, VU Station B 351592, 2301 Vanderbilt Place; carol.rubin@vanderbilt.edu.
‡Professor Emeritus, Department of Mechanical Engineering.

Background

References 1–9 contain analytical studies of the stresses in adhesive lap joints, and papers in Refs. 10–19 present finite element analyses for high-modulus adhesive lap joints. All of these papers concentrate on in-plane continuous adhesive lap joints without rivets. They use methods such as continuum mechanics and finite elements to determine the stresses in the adhesive layer, which is treated as thick with high modulus. Only Baker and Hatt[13] treat a thin adhesive layer, treating the layer as a combined tension and shear linear spring element using finite element analysis. Pascal et al.[20] used finite element methods to determine the stresses in a lap joint with a low-modulus adhesive; the adhesive is treated as thick and does not represent eccentric tensile loading of the joint. References 21–25 concentrate on riveted lap joints without adhesive polymer sealants. References 26 and 27 study the effects of thick layers of high-modulus adhesives, such as epoxies, on riveted lap joints. Kamnerdtong[28] and Fongsamootr[29] measured the mechanical behavior of thick[28,29] and thin[30,31] layers of low-modulus sealants in the normal and shear directions. This behavior is nonlinear and pressure dependent.

Method

In the present context the term sealant is used to refer to nonlinear, rubberlike, low-modulus, sticky polymers with pressure-dependent shear properties. The term adhesive is used to refer to linear, higher-modulus polymers. The unriveted and riveted lap joints that are analyzed and measured in this work are fastened or sealed with a low-modulus sealant. TALA can treat the mechanical effects of both sealants and adhesives. Because their effects on lap joints are qualitatively similar, the terms sealant and adhesive are used interchangeably for TALA based on the current context.

In this study a solid thin sealant element is converted to spring elements connecting two contacting surfaces, eliminating solid-element representation of the sealant layer in the finite element models as shown in Fig. 1. The general idea of TALA is that each pair of coincident nodes between two contacting surfaces in the finite element models is connected by spring elements (defined as SPRING2 elements in ABAQUS). The mechanical behavior of the springs must be defined in local normal and local shear directions in the finite element models. The stresses and strains in the springs are converted to forces and displacements interacting between the two contacting surfaces. The properties

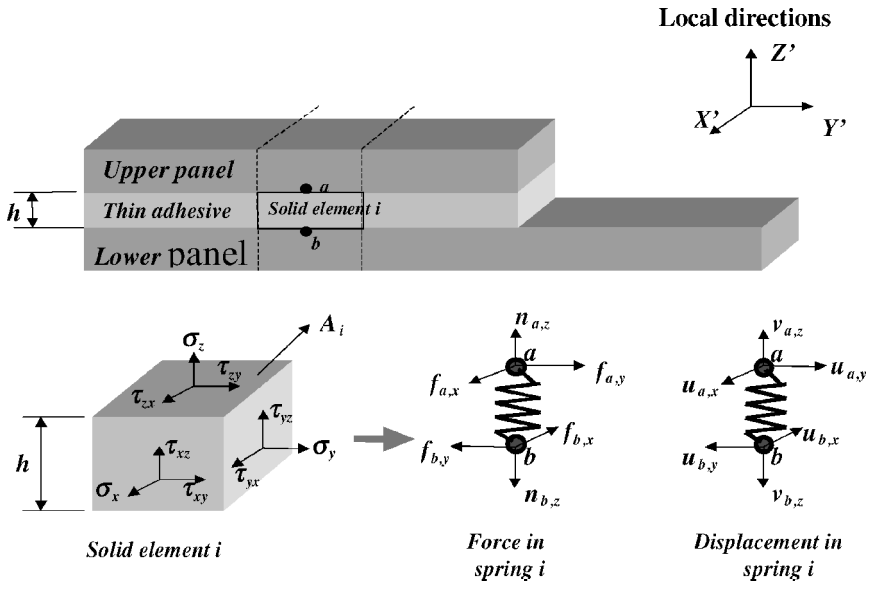

Fig. 1 Schematic of spring representation of solid adhesive element.

of the adhesive are treated as isotropic and time and load rate independent.

Conversion of Adhesive Solid Element to Spring Element for Two-Dimensional Models

Two methods[32] are used for changing the solid adhesive element to spring elements; each method requires different values for A_i as described in the following subsections.

One Solid Element to One-Spring Method

This method is used to change one solid adhesive element to one spring as shown in Fig. 2a. It changes adhesive element i (bonding elements U_i and L_i) to spring S_i. A spring S_i is composed of two spring elements, connecting node u_i with node l_i, using one normal and one shear spring element. The area for spring S_i is equal to

$$A_i = w_i \cdot d \tag{1}$$

where w is the width of each element (in y' direction) along the interface line and d the depth of each element (in x' direction); this value is always one unit for two-dimensional plane strain.

One Solid Element to Three-Spring Method

This method is used to change one solid adhesive element to three springs, as shown in Fig. 2b. It changes adhesive element i (bonding panel elements U_i and L_i) to springs S_{i-1}, S_i and S_{i+1}. The spring S_{i-1} is composed of two spring elements connecting node u_{i-1} with node l_{i-1}, using one normal and one shear spring element. The area for spring S_{i-1} is

$$A_{i-1} = [(w_{i-1}/4) + (w_i/4)] \cdot d \tag{2}$$

where w is the width of each element (in y' direction) and d depth of each element (in x' direction). Similarly, the spring S_i is composed of two spring elements connecting node u_i with node l_i in the normal and shear directions. The area for spring S_i is

$$A_i = (w_i/2) \cdot d \tag{3}$$

The area for spring S_{i+1} is

$$A_{i+1} = [(w_{i+1}/4) + (w_i/4)] \cdot d \tag{4}$$

Conversion of Adhesive Solid Element to Spring Element for Three-Dimensional Models

For the three-dimensional finite element model the change from thin solid adhesive elements to spring elements is based on the same idea used for the two-dimensional problem; however, the area for each spring A_i must be calculated differently. Figure 3 shows the features of the three-dimensional finite element with elements U_i

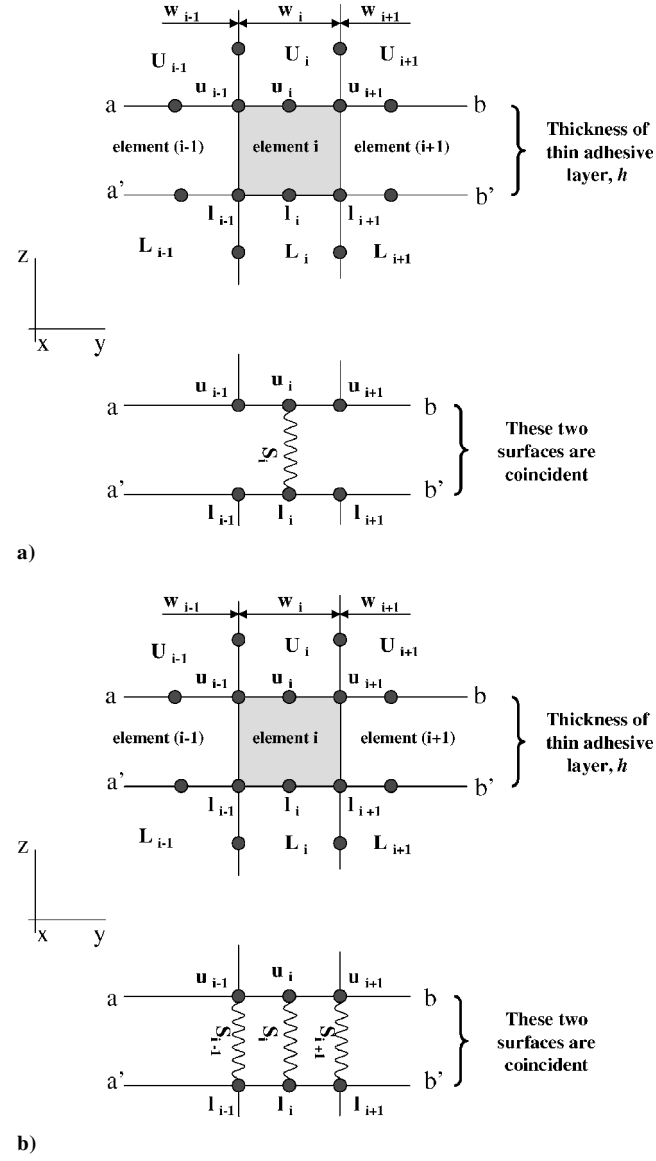

Fig. 2 Schematic of springs between two interfacing surfaces for two-dimensional finite element model using a) one and b) three springs.

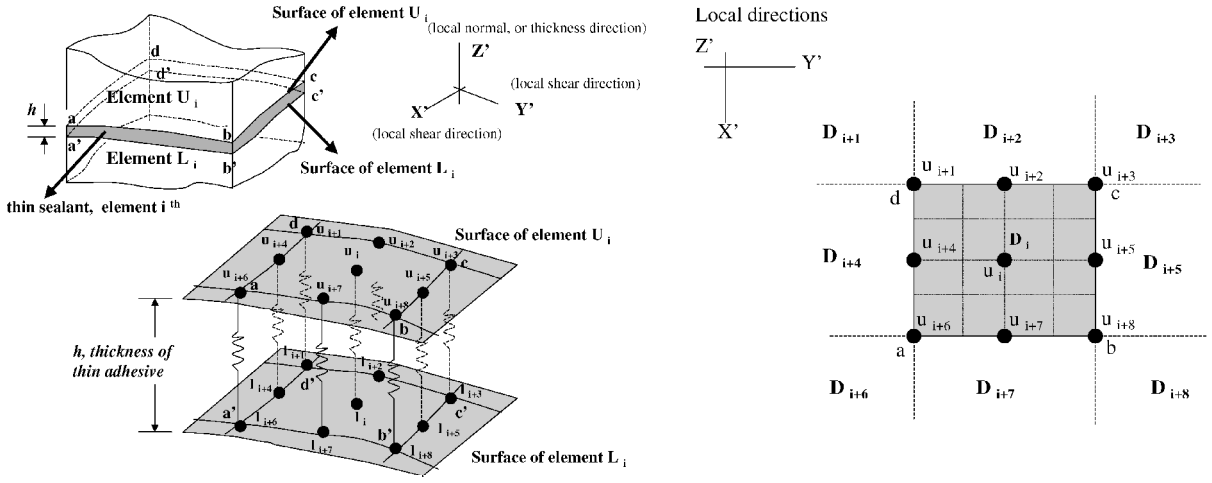

Fig. 3 Schematic for representing solid adhesive element with spring elements.

Table 1 Formulation for calculating the spring area for the three-dimensional model

Spring	Spring area
S_i	$A_i = (D_i)/16$
S_{i+1}	$A_{i+1} = (D_i)/16 + (D_{i+1})/16 + (D_{i+2})/16 + (D_{i+4})/16$
S_{i+2}	$A_{i+2} = (D_i)/8 + (D_{i+2})/8$
S_{i+3}	$A_{i+3} = (D_i)/16 + (D_{i+2})/16 + (D_{i+3})/16 + (D_{i+5})/16$
S_{i+4}	$A_{i+4} = (D_i)/8 + (D_{i+4})/8$
S_{i+5}	$A_{i+5} = (D_i)/8 + (D_{i+5})/8$
S_{i+6}	$A_{i+6} = (D_i)/16 + (D_{i+4})/16 + (D_{i+6})/16 + (D_{i+7})/16$
S_{i+7}	$A_{i+7} = (D_i)/8 + (D_{i+7})/8$
S_{i+8}	$A_{i+8} = (D_i)/16 + (D_{i+5})/16 + (D_{i+7})/16 + (D_{i+8})/16$

and L_i bonded by a thin adhesive layer. Nodes on surface *a-b-c-d* of element U_i and *a'-b'-c'-d'* of element L_i are coincident. The thin adhesive element i bonding the two surfaces of elements U_i and L_i are changed to nine springs for use with 27 node isoparametric elements, etc. Spring S_i connects nodes u_i and l_i together, etc. Each spring is composed of three spring elements, one normal spring, and two shear springs. Areas D_i through D_{i+8} are shown schematically in Fig. 3 and are used to obtain A_i through A_{i+8} for the springs, as shown in Table 1.

Conversion of Stress–Strain Relationship to Force–Displacement Relationship for Thin Layer

In this study the adhesive layer is assumed very thin. Thus, the stresses σ_x, σ_y, τ_{xz}, τ_{xy}, τ_{yz}, τ_{yx}, γ_{xz}, γ_{xy}, γ_{yz}, and γ_{yx}, as shown in Fig. 1, are neglected using TALA. Only σ_z, τ_{zx}, and τ_{zy} act between the two nodes. The normal stress σ_z is changed to normal force, whereas the shear stresses τ_{zx}, τ_{zy} are changed to shear force in each spring element. The normal and shear strains ε_z, γ_{zy}, γ_{zx} are changed to normal and shear relative displacements in spring i.

The equations used for converting the stresses and strains in the solid element to forces and displacements in the spring element are presented next. In the normal direction (tension and compression spring), by Hooke's law,

$$\sigma_z = E^*(\varepsilon_z) \tag{5}$$

$$(n_{a,z} + n_{b,z})/A_i = E^*(\varepsilon_z) \tag{6}$$

$$\varepsilon_z = (v_{a,z} + v_{b,z})/h \tag{7}$$

$$(n_{a,z} + n_{b,z}) = [E^*(A_i/h)]^*(v_{a,z} + v_{b,z}) \tag{8}$$

$$(n_{a,z} + n_{b,z}) = K_n^*(v_{a,z} + v_{b,z}) \tag{9}$$

$$F_{n,i} = K_{n,i} * v_{n,i} \tag{10}$$

$$K_{n,i} = E^*(A_i/h) \tag{11}$$

where $n_{a,z}$ and $v_{a,z}$ are the relative force and displacement at node a in the z direction, h is the adhesive thickness, $F_{n,i}$ is the normal force transmitted in spring element i, $K_{n,i}$ is the local stiffness of spring element i in the local normal direction, and E is the elastic modulus of the adhesive. In the shear direction (shear spring), in the x'–y' plane τ_{zx} and τ_{zy} would be the same for an isotropic material.

$$\tau_{zx} = G^*(\gamma_{zx}) \tag{12}$$

$$(f_{a,x} + f_{b,x})/A_i = G^*(\gamma_{zx}) \tag{13}$$

$$\gamma_{zx} = (u_{a,x} + u_{b,x})/h \tag{14}$$

$$(f_{a,x} + f_{b,x}) = [G^*(A_i/h)]^*(u_{a,x} + u_{b,x}) \tag{15}$$

$$(f_{a,x} + f_{b,x}) = K_f^*(u_{a,x} + u_{b,x}) \tag{16}$$

$$F_{f,i} = K_{f,I}^* u_{f,i} \tag{17}$$

$$K_{f,i} = G^*(A_i/h) \tag{18}$$

where $f_{a,x}$ and $u_{a,x}$ are the relative shear force and displacement at node a in the x direction, $F_{f,i}$ is the shear force transmitted in spring element i, $u_{f,i}$ is the relative displacement of spring element i in the shear direction, $K_{f,i}$ is the local stiffness of spring element i in the shear direction, and G is the shear modulus of the adhesive.

For the case of a linear material, the values of $K_{n,i}$ and $K_{f,i}$ can be defined directly for a spring element i in the normal and shear directions. However, for a nonlinear material $K_{n,i}$ and $K_{f,i}$ vary. Then, define the nonlinear behavior for spring element i, pairs of force-relative displacement values are required over a sufficiently wide range of relative displacement values. For more information about defining spring properties, see Ref. 33.

Mechanical Behavior of Thin Sealant Layer

To use TALA and ABAQUS to simulate the mechanical behavior of the layer, the actual behavior of the thin sealant coating must be fully described. Low-weight aerospace sealant (PR-1776 B-2 Model 654) supplied by PRC-DeSoto International, Inc., is used in this study. In the normal direction the stress–strain relationship for a thin sealant coating layer of this material subjected to uniaxial static tension and compression loading is obtained by Fongsamootr,[30] as shown in Fig. 4. In the shear direction data for the sealant, subjected to combined torsion and compression loading, are obtained by Kamnerdtong,[31] as shown in Fig. 5.

Shear Spring Dependence of Contact Pressure

A procedure for the determination of the pressure-dependent stress–strain behavior for the shear spring is described here. Figure 5 gives shear stress–strain relationships for various pressures (in-between values are obtained through interpolation). To start with, the contact pressure is assumed to be zero. After the first ABAQUS run the normal force in each spring is output (DAT file). If the value of the normal force $F_{n,i}$ is tensile or zero, the force–displacement

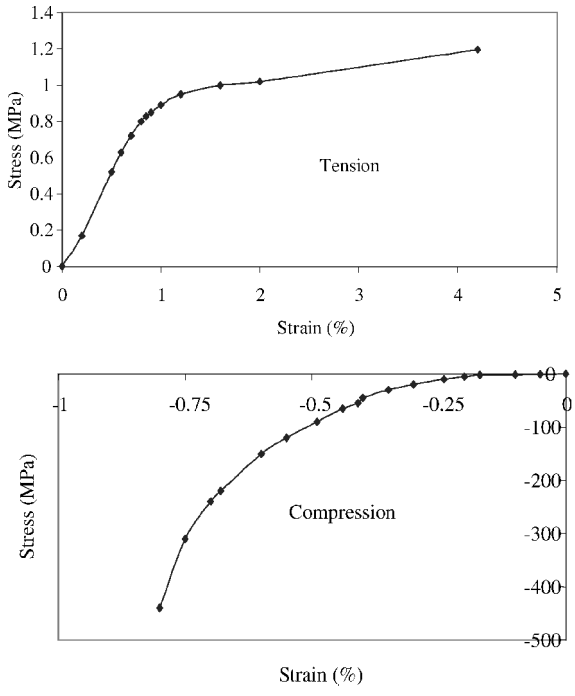

Fig. 4 Uniaxial stress–strain relationship for a thin sealant (PR-1776) coating layer 170 μm thick.

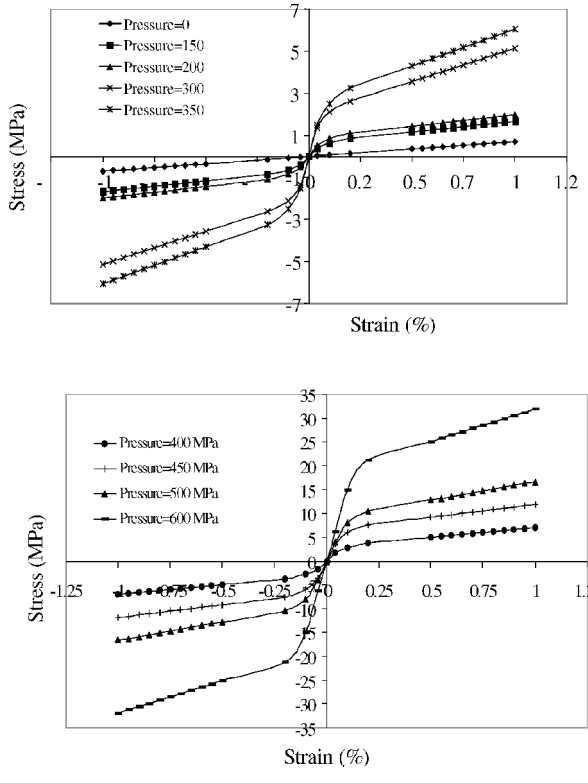

Fig. 5 Shear stress–strain relationships for a thin sealant coating layer 100 mm thick for contact pressure from a) 0–350 and b) 400–600 MPa.

relationship for the shear spring is kept constant. This is because shear behavior data were not obtained as a function of tension; thus, the assumption is made that tension has a negligible affect on the sealant shear properties. If the value of the normal force $F_{n,i}$ is compressive, the compressive force is divided by the small area A_i to get the new value of the contact pressure P_i for that spring element. Then, for the next run the shear spring of that element is redefined to have a new shear force–displacement relationship from the new contact pressure. Using this idea, the model is run repeatedly, and the shear spring is redefined until the new contact pressure and previous contact pressure for each spring converge. EXCEL is used to provide a new input file for each new run and to define new shear spring pressure dependence following P_{inew} for each spring.

Validations and Applications of TALA

Analytical Validation: Finite Element Model of Cornell's Work

In Cornell's work[9] the brazed tab specimen (including the effect of fillet), as shown in Fig. 6a, was used to determine the stresses in a braze bonding layer. The steel tab and steel base-bar are bonded using a braze layer. In this analysis braze is acting as a linear high-modulus adhesive. The brazed tab specimen is configured as a cantilever beam. The bonding layer is assumed to consist of an infinite number of linear tension and shear springs.

In the present study the brazed tab specimen is created using PATRAN as a two-dimensional plane-strain finite element model with no fillet as shown in Fig. 6b. The model uses 150 elements for the steel tab and 570 elements for the steel base bar (all ABAQUS CPE8 elements). The specimen is loaded in pure bending. The Young's modulus and Poisson's ratio for steel are 206 GPa (30×10^6 psi) and 0.3, respectively. The braze bonding layer thickness of 0.254 mm (0.01 in.) with length of 50.8 mm (2.0 in.) is transformed to spring elements using TALA. The SPRING2 ABAQUS element is employed to simulate the force–displacement relationship for a braze solid bonding layer. The TALA method is employed to change the braze solid bonding layer to 51 linear tension–compression spring elements and 51 linear shear spring elements connecting the lower surface of the tab and the upper surface of the base bar (along line a-b as shown in Fig. 6b). The shear spring behavior is assumed to be independent of contact pressure. The Young's modulus and shear modulus of braze are 103 GPa (15×10^6 psi) and 34.5 GPa (5×10^6 psi), respectively.

To verify TALA, the nondimensional stress distributions $\sigma_y/\sigma_{\max}$ and $\tau_{xy}/\sigma_{\max}$ in the braze bonding layer are obtained and compared

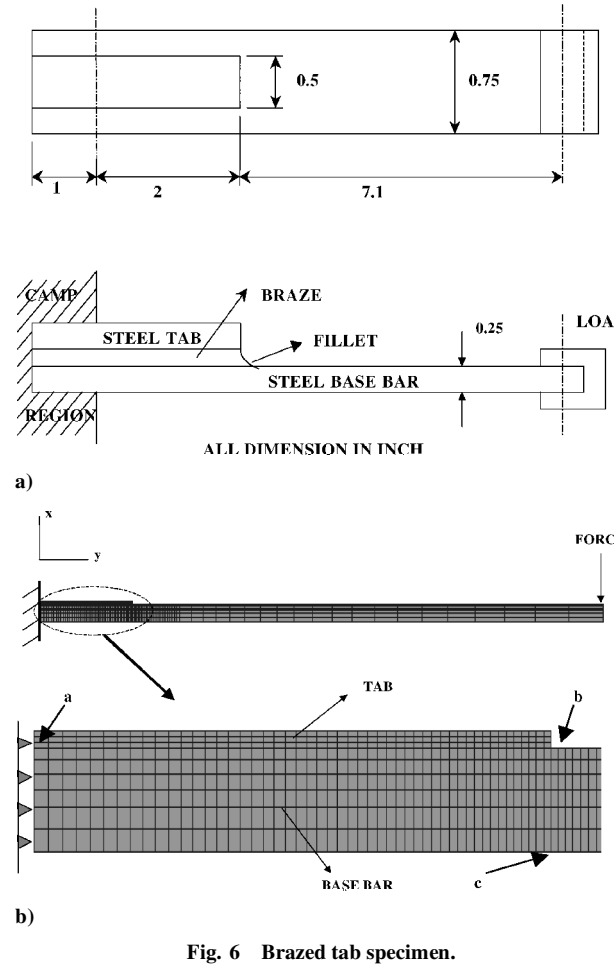

Fig. 6 Brazed tab specimen.

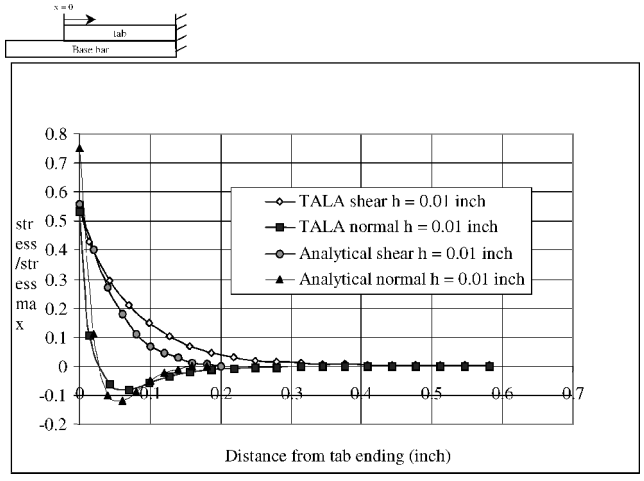

Fig. 7 Normal and shear stress in braze bonding layer: *h* (thickness of braze layer) = 0.01 in. (0.254 mm).

with the analytical closed-form solution obtained by Cornell.[9] In this case σ_{max} is the maximum nominal bending stress occurring in the base bar at the end of the tab bending (point c as shown in Fig. 6). To obtain the stresses in the braze bonding layer using TALA, the normal force and shear force reported in the ABAQUS output file for each spring element are divided by the calculated area of each spring element and then compared in Fig. 7.

It can be seen from Fig. 7 that the Cornell and TALA analyses are essentially in agreement. The shapes of the curves of τ_{xy}/σ_{max} and σ_y/σ_{max} are almost the same; there is a small difference in the magnitudes at 1.27–7.62 mm (0.05–0.3 in.) from the tab ending. The stresses reach zero at 7.62 mm (0.3 in.) from the tab ending using TALA, whereas Cornell's stresses become zero at 5.08 mm (0.2 in.). Small differences in the magnitude and location of the stresses are because TALA does not include the braze layer fillet at the tab ending.

Analytical Validation: Finite Element Model of Baker and Hatt's Work

Baker and Hatt[13] use a linear elastic finite element analysis to evaluate the behavior of a two-dimensional thin adhesive joint bonding two dissimilar materials. The adhesive layer is treated as a thin and linear high-modulus material. This special element acts like a combined normal and shear spring between two plates and is independent of the contact pressure. This method is not the same as TALA; the difference lies in the definition of the connection between coincident and adjacent nodes.

In the present study the adhesive lap joint of Baker and Hatt, shown in Fig. 8a, is created using PATRAN as a two-dimensional plane-strain finite element model (Fig. 8b). There are 500 elements for aluminum and 500 for steel (all CPE8). The adhesive single lap joint, which acts only along d-e, is subject to a tension load P_0 at face g-h and constrained in all directions along face a-b. To maintain pure shear in the adhesive layer, the face b-f-h is restrained in the y direction. The material properties are $E_{aluminum} = 69$ GPa (10×10^6 psi), $\nu_{aluminum} = 0.3$, $E_{steel} = 206$ GPa (30×10^6 psi), $\nu_{aluminum} = 0.3$, $E_{adhesive} = 31$ GPa (4.45×10^5 psi), and $G_{adhesive} = 11.3$ GPa (1.65×10^5 psi).

Within TALA the adhesive layer is transformed to 50 linear tension-compression and 50 linear shear spring elements connecting the lower surface of steel to the upper surface of aluminum (along line d-e as shown in Fig. 8b) using the one spring method, as shown in Fig. 2a. The shear spring behavior is assumed to be independent of contact pressure. Stress distributions along the adhesive layer for thicknesses of 0.01L and 0.001L are obtained.

The TALA analysis results are compared with the results of Baker and Hatt in Fig. 9 showing normalized shear stress τ/p_0, where p_0 is the applied load (see Fig. 8), along the overlapping length x/l for two different adhesive thicknesses. In this study there are peak shear stresses at the left and right ends of the overlapping length (at $x/l = 0$ and 1). These stresses are not equal because the upper and

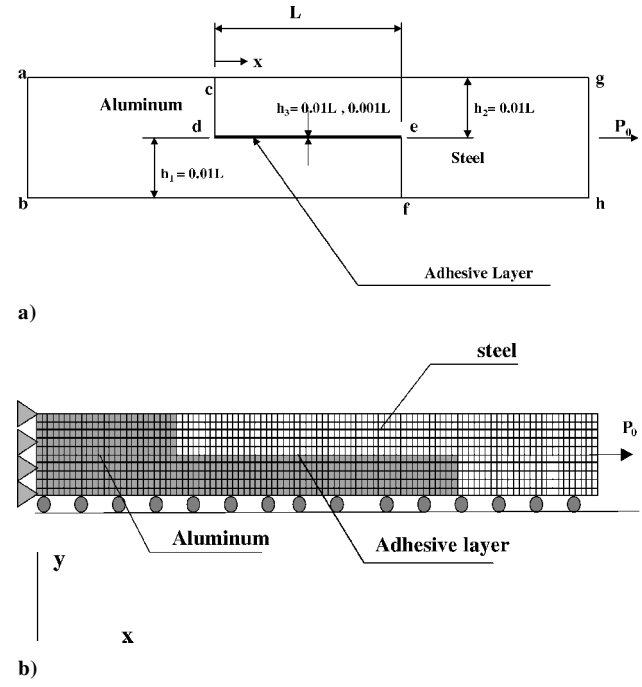

Fig. 8 Baker and Hatt's adhesive single lap-joint model.

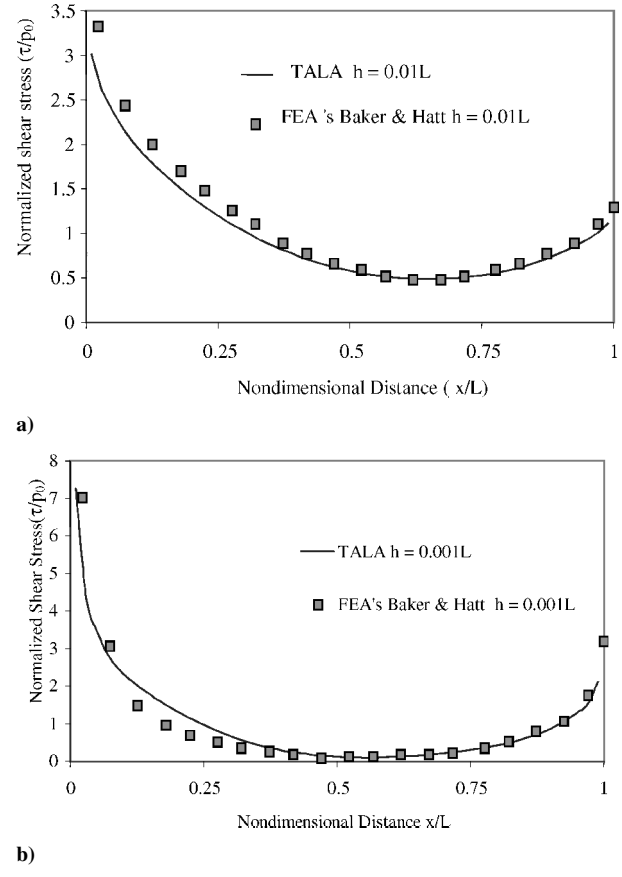

Fig. 9 Shear stress in thin adhesive layer.

lower panels are different materials. The shear stress distribution is not symmetrical; the lowest shear stress is located to the right of the middle of the overlapping length. The peak shear stress at the ends increases when the thickness of the adhesive is decreased; on the other hand, the lowest shear stress decreases when the thickness of the adhesive is decreased.

The TALA analysis results are in agreement with Baker and Hatt's analysis in both shape and magnitude along the overlapping length.

Experimental Validation: Design of Experiments

Experiments were designed to validate the TALA approach for thin low-modulus sealants. The sealants are modeled as nonlinear in the normal and shear directions, with pressure-dependent properties. Thin layers of adhesive sealant polymer (PRC-Desoto PR-1776 B-2 Model 654 currently used as sealant coatings in aircraft structures) were inserted in the test specimens. Test specimens of adhesive lap joints, adhesive stepped lap joints, and standard riveted plus adhesive lap joints were used. In-plane and out-of-plane displacements of the joints were obtained.

Joint Preparation

The test pieces consisted of 7075-T6 aluminum alloy panels and 2117-T4 aluminum alloy rivets. Prior to applying the sealant layer, the surfaces were anodized and coated with polyurethane. This surface preparation is typical for sealing joints in aircraft structures. All test specimens were sent to Aero-Structure, Inc., Nashville, Tennessee, for surface preparation. For the adhesive and adhesive stepped lap joints the sealant (PR-1776) was applied along the overlapping length of 30.6 mm. For the sealed riveted lap-joint test specimen the thin sealant layer was applied at all contacting surfaces initially, and then the rivet was inserted. The rivet was installed slowly, and the upsetting process was terminated when the rivet shank contacted the panels, in order to minimize clamping and rivet-hole interference. It was impossible to maintain a constant sealant layer thickness for all of the specimens because of difficulties in controlling the amount of sealant applied.

After fabrication the specimens were allowed to cure for approximately 14 days. The adhesive and adhesive stepped lap-joint specimens were clamped to maintain the layer thickness during curing. To determine the sealant layer thickness, the total thickness of the joint (upper and lower panel and sealant layer) was measured using a micrometer; the thickness of the upper and lower panels was subtracted from the total. Several measurements were taken, and average values were used. The thicknesses of the sealant in the adhesive and adhesive-stepped lap joints are $\sim$125 and $\sim$60 μm, respectively, the same as used in the finite element models. For the sealed riveted lap joint the layer was found to be $\sim$180 μm thick. The sealant layer between the rivet and panels is assumed to be very thin compared to the sealant between the panels.

Test Configurations

The tests were performed on an MTS 809 Axial-Torsion Material Test System. The specimens were subjected to quasi-static tensile loading. During the tests, the magnitude of the applied load was recorded, and in-plane strain across the overlapping length was measured with an extensometer. To obtain the out-of-plane displacements for each joint, two dial gauges were placed along the centerline of the joint. The in-plane and out-of-plane displacements measured from the experiment are compared at the same loading as used in the finite element models, as shown in Table 2.

Experimental Validation: Finite Element Models Using TALA

Adhesive Lap Joint

The upper schematic in Fig. 10 shows the geometry of an adhesive lap joint; Fig. 11a shows the two-dimensional plane-strain finite element model of the same joint (developed in PATRAN); 201 ABAQUS CPE8 elements are used for each panel. The upper and lower panel material is aluminum alloy (T-6 7075, $E_{\text{aluminum}} = 70$ GPa, and $\nu = 0.3$). The end of the lower panel is constrained in all directions, whereas the end of the upper panel is constrained only in the y direction and loaded with various nominal static stresses in the x direction. This loading and the adhesive thickness used in the finite element model are the same as those used in the test specimens. The 125-μm-thick sealant is used to bond the two panels along an overlap length of 30.6 mm. The one spring method for TALA is used along line a-b, with 17 nonlinear normal and 17 nonlinear shear springs (SPRING2). The force and displacement data pairs for each nonlinear spring, based on the actual stress–strain relationships as shown in Figs. 4 and 5, are defined in the input file.

Adhesive-Stepped Lap Joint

The lower schematic in Fig. 10 shows the geometry of an adhesive stepped lap joint; Fig. 11b shows the two-dimensional plane-strain finite element model of the same joint; 195 ABAQUS CPE8 elements are used for each panel. The upper and lower panel material is aluminum alloy (T-6 7075, $E_{\text{aluminum}} = 70$ GPa, and $\nu = 0.3$). The end of the upper panel is constrained in all directions, whereas the end of the lower panel is constrained only in the y direction and loaded with various nominal static stresses in the x direction. The loading and the sealant thickness used in the finite element model are the same as those used for the test specimens. The 60-μm-thick sealant (PR-1776) is used to bond the stepped lap joint along the

Table 2 Test nominal tensile stress used in the finite element models

Specimen	σ_1, MPa	σ_2, MPa	σ_3, MPa
Adhesive lap joint	3.81	12.36	17.63
Adhesive stepped lap joint	14.43	52.66	78.43
Riveted lap joint	16.69	37.64	62.66

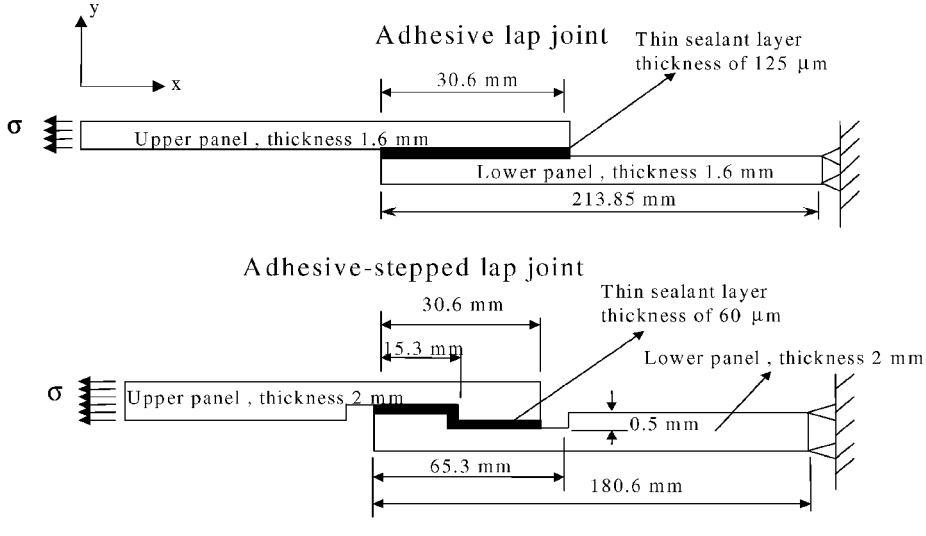

Note: width = 80 mm for both models

Fig. 10 Geometry of adhesive and adhesive-stepped lap-joints test specimens.

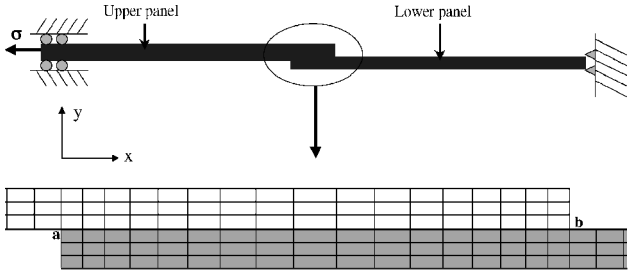

Fig. 11a Finite element model of adhesive lap joint.

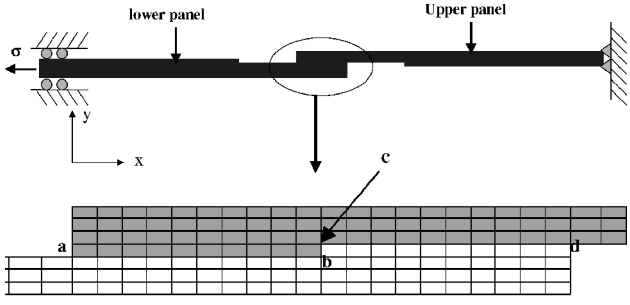

Fig. 11b Finite element model of adhesive-stepped lap joint.

overlapping length of 30.6 mm along lines a-b, b-c, and c-d. TALA is used along this contact length with 20 nonlinear normal and 20 nonlinear shear springs (SPRING2). The three-springs method is used for the connection. The force- and-displacement data pairs for each nonlinear spring are based on the actual stress–strain relationships, as shown in Figs. 4 and 5.

The values of in-plane and out-of-plane displacements of the joints as measured in the experiments are compared with finite element results.

Single Rivet-Row Lap Joints

Finite element models for studying the effect of a thin sealant layer on single rivet-row lap joints (standard and countersunk riveted joints without clamping or interference) are presented here. The finite element models for standard and countersunk riveted lap joints are treated in different configurations: 1) an infinitely wide multiriveted lap joint (Fig. 12) and 2) a finite-width single-rivet lap joint (Fig. 13).

The finite element models of multiriveted lap joints, having infinite width and no free lateral edges, were created by Iyer.[25] They are used to represent the riveted lap joints that are generally used in actual aircraft fuselages. The finite element models of finite-width single-rivet lap joints are used to represent the lap joints used as test specimens in the laboratory (Fig. 13). The difference between the multiriveted and single-rivet finite element models is that the latter has one lateral edge free. The single-rivet lap joint model is used as

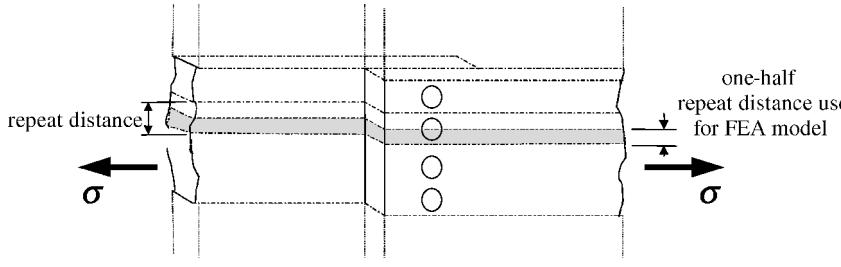

Fig. 12a Multiriveted, single rivet-row lap joint.

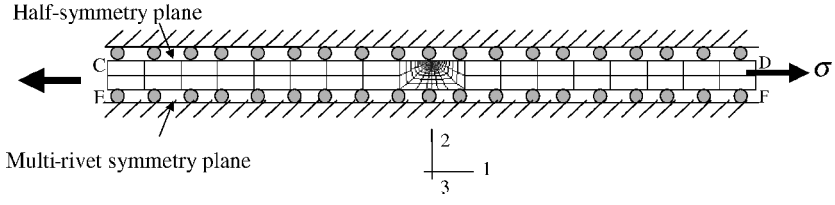

Fig. 12b View of the mesh. The overall length of the model is 306 mm; the length of the overlap is 30.6 mm; and the width of the model (half the repeat distance) is 15.3 mm.

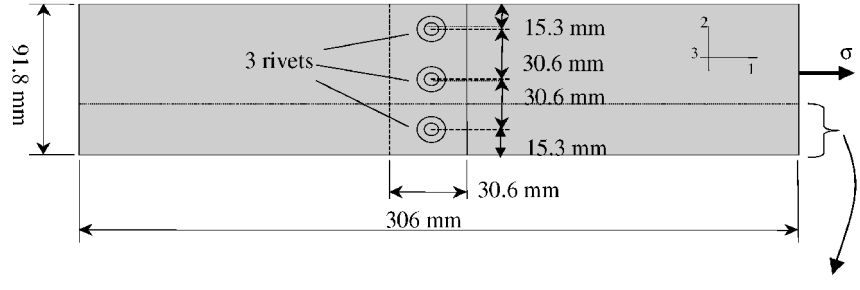

Fig. 13a Three-riveted lap-joints test specimen.

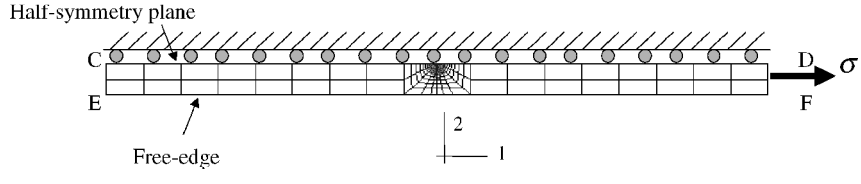

Fig. 13b Finite element model of one-riveted lap joint.

an approximation of the three-rivet test specimens. It would be much more difficult to model all three rivets using finite element analysis, requiring much more CPU time and creating mesh-refinement problems. In previous works,[34,35] it was found that the compliance and stress concentration factors in riveted lap joints are elevated by a lateral free edge. Table 3 indicates the finite element models used in this study.

Table 3 Finite element models

Model	Description
A-0-m[a,b,c]	Standard single rivet-row, no-adhesive
B-0-m[d]	Countersunk single rivet-row, no-adhesive
A-1-m[e]	Standard single rivet-row, plus-adhesive
B-1-m	Countersunk single rivet-row, plus-adhesive
A-0-s[f]	Standard single rivet-row, no-adhesive
B-0-s	Countersunk single rivet-row, no-adhesive
A-1-s	Standard single rivet-row, plus-adhesive
B-1-s	Countersunk single rivet-row, plus-adhesive

[a] A = noncountersunk rivet.
[b] 0 = no adhesive.
[c] m = multiple rivets.
[d] B = countersunk rivet.
[e] 1 = adhesive.
[f] S = single rivet.

Experimental Validation: Comparisons of Experimental and Finite Element Results

Figure 14 shows a comparison of the experimental and finite element relative in-plane and out-of-plane displacement results at the same tensile loads. The calculations agree with the measurements for small applied loads. Small divergences for high loads are probably caused by stress relaxation in the sealant layer during the period of time that the displacements were held constant to allow

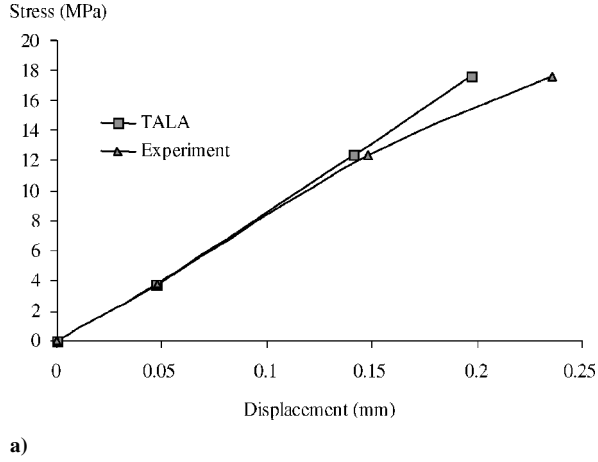

a)

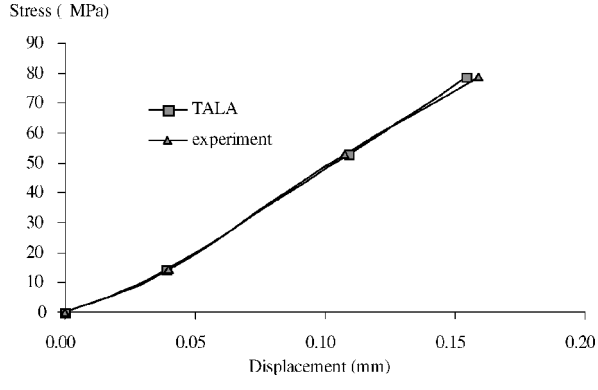

b)

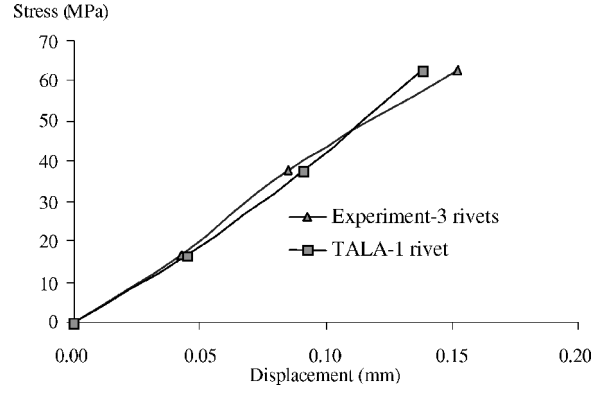

c)

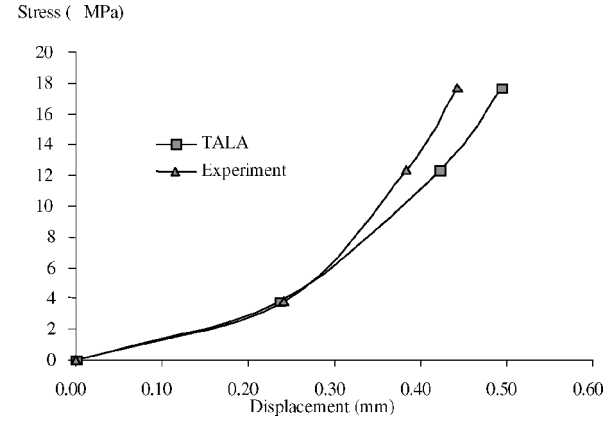

d)

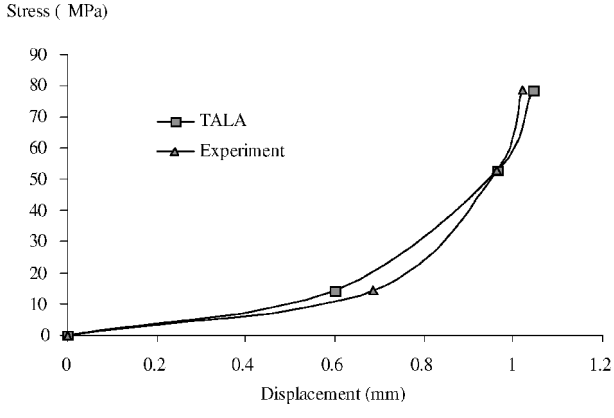

e)

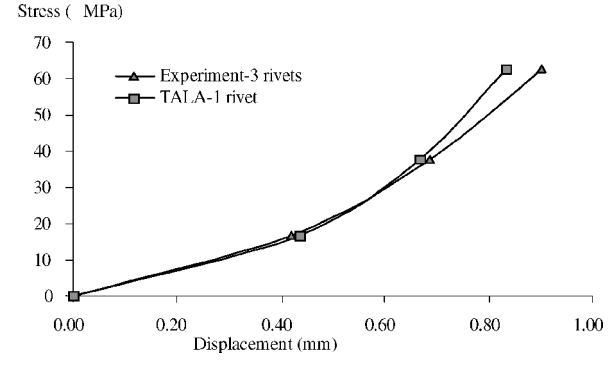

f)

Fig. 14 Comparison of experimental and finite element relative in-plane and out-of-plane displacement results at the same tensile loads: a), b), and c) compare the measured and calculated in-plane displacement-nominal stress relation for adhesive lap joint, adhesive stepped lap joint, riveted lap joint, respectively; and d), e), and f) compare the measured and calculated out-of-plane displacement-nominal stress relation for adhesive lap joint, adhesive stepped lap joint, riveted lap joint, respectively.

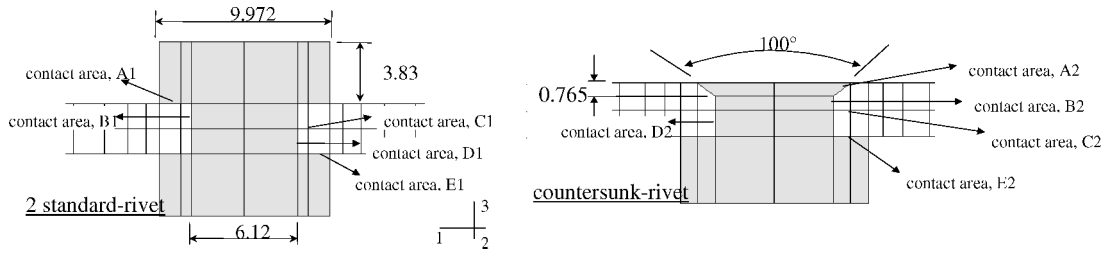

Fig. 15 Dimensions of rivets and detail of contact areas.

for reading of the dial gauges. The load-displacement relationship obtained from the three rivet lap joint test specimens is compared with the finite element calculations for the one-rivet lap joint (see Fig. 13). This might cause slight discrepancies between the measured and calculated displacements.

Analytical Applications: Multiriveted Lap Joints (A-0-m, A-1-m, B-0-m, and B-1-m)

The three-dimensional finite element models A-0-m and B-0-m were created by Iyer[25] (with no sealant at interfacing surfaces) using a reduced applied load (62.66 MPa instead of 125 MPa). The model geometry consists of two partially overlapping panels fastening by a rivet, as given in Fig. 12. It represents one-half unit of a multiriveted, single-row, long panel extending in the positive and negative two directions. The repeat distance between successive units is 30.6 mm. A nominal static stress of 62.66 MPa is applied at the end of the upper panel at face DF in the 1 direction. The face CE at the lower panel is fixed in the 1 direction, while faces CD and EF are fixed in the 2 direction. To prevent rigid-body rotation, faces DF and CE are fixed in the 3 direction.

The panel and rivet are aluminum alloy T6-7075 and T4-2117, respectively. Details of the rivet geometries are presented in Fig. 15. The material behavior of aluminum is elastic. ABAQUS C3D27, 27-node brick elements, and C3D15V 15- to 18-node triangular prisms are used for the panels and rivets, respectively. The finite element meshes typically consist of 3171 user-defined nodes, 252 user-defined solid elements, and 609 internally generated contact elements. A friction coefficient of 0.2 was applied at all contacting surfaces.

To create the A-1-m and B-1-m models, the A-0-m and B-0-m models are modified by replacing the frictional resistance at all of the contacting surfaces with TALA. TALA is applied at the contacting surfaces A1, B1, C1, D1, and E1 (as indicated in Fig. 15) for the standard riveted lap-joint model and at the contacting surfaces A2, B2, C2, D2, and E2 for the countersunk riveted lap-joint model. 693 normal springs and 1386 shear springs are used for standard riveted lap joint. 651 normal springs and 1302 shear springs are used for countersunk riveted lap joint. The pressure-dependent shear property is taken into account in the analysis. The sealant (PR-1776) is used to bond all contacting surfaces in the joints. The thickness of the adhesive layer is 180 μm (obtained from the test specimen) between the upper and lower panels (at contact areas C1 and C2). It is assumed that the adhesive layer around the rivet is very thin (9 μm); this value was obtained by matching the finite element and experimental results.

Analytical Applications: Single Rivet-Row Lap Joints (A-0-s, A-1-s, B-0-s, and B-1-s)

To create the A-0-s, B-0-s, A-1-s, and B-1-s models, the A-0-m, B-0-m, A-1-m, and B-1-m are modified by removing the constraints on face EF in the 2 direction. All of the other configurations for the single-rivet lap joint models are the same as they were for the multiriveted lap joints. Figure 13 shows the details of the single-rivet lap-joint configuration.

The local mechanical parameters [excess compliance, rivet tilt, in-plane, and out-of-plane slip at certain interesting points (a, a', a", b, b', b", c, c', c", d", g, and h), as shown in Fig. 16a, peak tensile stress in panel hole, peak contact pressure, panel–panel separation

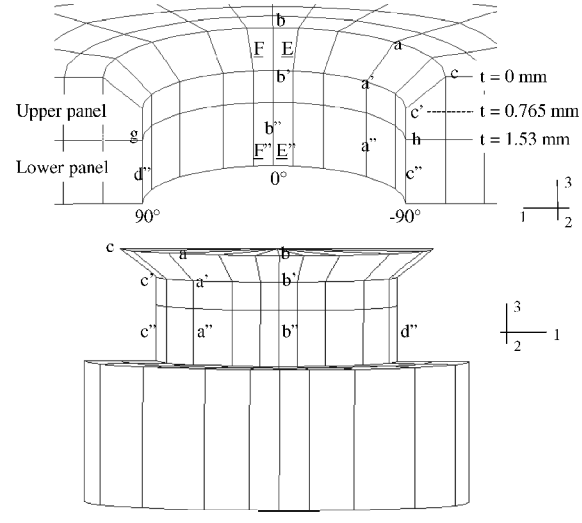

Fig. 16a Map of important locations for in-plane and out-of-plane slip.

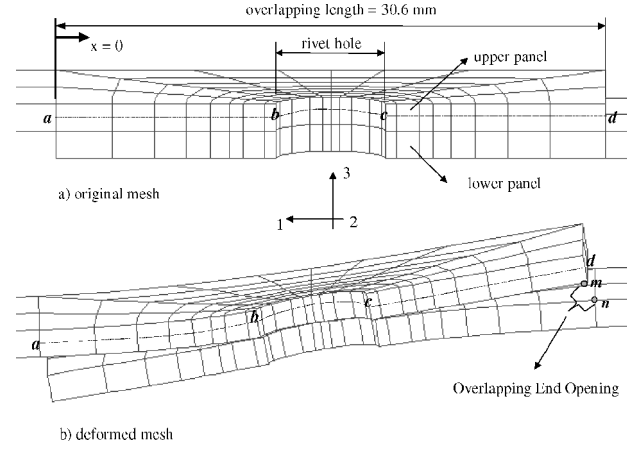

Fig. 16b Illustrations of overlapping end opening and the curvature line a-b-c-d on the upper panel.

(observing from points m and n in Fig. 16b), stresses in the panel and in the rivet, and panel bending (observed from curvature line a-b-c-d in Fig. 16b) for each model] are examined and compared at the same tensile loading. The configuration and definition of each of these parameters are treated next. The excess compliance is defined as $C = C' - C''$ (Ref. 33). The C' is the assembly compliance, that is, the ratio of the net extension δ to load per repeat distance P ($C' = \delta/P$). $C'' = 93.4$ m/GN is the compliance of a continuous panel having the same length L as the model joint (length of two panels minus the overlap) and the same cross-sectional area A and elastic modulus E as a single panel.

Results of Analytical Application: Sealant Effects on Lap Joints

Table 4 shows the influence of the thin sealant layer on the distortion of the riveted lap joints. The sealant increases excess

Table 4 Influence of a thin sealant layer on the distortion of infinitely wide multiriveted and finite width single-riveted lap joints

		Standard riveted lap joints				Countersunk riveted lap joints			
		Multiple rivet		One rivet		Multiple rivet		One rivet	
Feature	Location	A-1-m	A-0-m	A-1-s	A-0-s	B-1-m	B-0-m	B-1-s	B-0-s
Excess compliance, m/GN	——	38.25	33.27	44.93	39.95	39.88	35.18	46.50	41.86
Rivet tilt, deg	——	2.46	2.52	2.47	2.52	2.74	2.82	2.77	2.84
Total in-plane slip at rivet–panel interface, mm	a	12.26	8.65	11.81	8.26	17.75	17.24	17.24	16.50
	a’	15.56	8.29	15.02	7.91	17.84	13.02	17.24	12.35
	a”	−29.00	−23.37	−30.41	−24.68	−29.27	−23.78	−30.50	−25.01
	b	26.60	21.50	26.60	21.40	32.50	30.20	32.90	30.30
	b’	31.70	22.90	31.60	22.50	38.90	34.10	38.80	33.80
	b”	−31.70	−22.90	−31.60	−22.50	−31.40	−23.20	−31.20	−22.90
Total in-plane slip at panel–panel interface, mm	g	67.80	46.60	68.80	47.50	84.70	76.80	84.70	78.10
	h	67.80	46.60	68.70	47.40	72.50	49.50	72.50	50.20
Total out-of-plane slip, mm	c	−29.72	−3.56	−29.37	−3.48	−27.50	−12.96	−27.00	−12.64
	c’	−31.20	−1.24	−30.83	−1.18	−20.93	−7.00	−20.60	−6.82
	c”	10.21	2.89	10.35	2.95	15.43	1.11	15.45	1.16
	d”	31.20	1.30	31.20	1.20	68.40	2.90	67.10	2.90
Peak tensile stress in elements adjacent to rivet hole, MPa	e	320.2	382.2	340.1	406.6	443.9	622.6	478.0	657.1
	e”	309.5	353.6	321.1	380.4	286.7	334.2	306.6	352.4
	f	309.5	353.6	321.1	380.4	443.9	615.8	475.5	655.3
	f”	320.2	382.2	340.1	406.6	295.5	362.7	311.9	379.3
SCF	——	5.1	6.1	5.4	6.5	7.1	10.0	7.6	10.5
Peak contact pressure, MPa	Shank hole	506.3	436.7	492.8	423.6	842.7	660.0	819.6	637.9
	Panel panel	11.0	434.1	10.9	420.9	9.0	409.3	8.9	410.1
	Panel–rivet head	245.1	244.7	245.5	244.5	284.8	545.3	286.6	542.3
Overlapping end opening, mm	m-n	0.11	0.24	0.11	0.24	0.12	0.29	0.13	0.29

Table 5 Stresses generated in rivets with and without a sealant layer

Model	Peak shank-hole compressive stress (S11), MPa	Peak shear stress (S13), MPa	Peak axial tensile stress (S33), MPa	Peak axial compressive stress (S33), MPa
Standard single rivet-row, no-adhesive (A-0-s, one-rivet)	−205.8	97.65	127.9	−157.1
Standard single rivet-row, plus-adhesive (A-1-s, one-rivet)	−246.0	112.4	86.1	−119.0
Standard single rivet-row, no-adhesive (A-0-m, multiple-rivet)	−212.1	105.6	127.2	−135.6
Standard single rivet-row, plus-adhesive (A-1-m, multiple-rivet)	−252.3	114.8	85.81	−111.3
Countersunk single rivet-row, no-adhesive (B-0-s, one-rivet)	−332.4	121.0	180.4	−191.2
Countersunk single rivet-row, plus-adhesive (B-1-s, one-rivet)	−364.2	130.0	87.28	−128.9
Countersunk single rivet-row, no-adhesive (B-0-m, multiple-rivet)	−314.4	123.7	181.9	−190.8
Countersunk single rivet-row, plus-adhesive (B-1-m, multiple-rivet)	−373.6	133.1	87.77	−107.8

compliance, in-plane slip at all interfacing surfaces, out-of-plane slip at all interfacing surfaces, and peak contact pressure at the rivet shank–panel interface for both standard and countersunk rivets. The sealant decreases the peak tensile stress in the panels, the peak contact pressure at the panel–panel interface, and panel–panel separation (see the last row of Table 4) for standard and countersunk rivets. The stress concentration factor (SCF = axial stress/applied nominal stress) decreases about 17 and 28% for standard and countersunk, respectively. The SCF and peak tensile stress are located at the bottom surface of the upper-panel hole (element E and F in Fig. 16a). The excess compliance and peak tensile stress in multiriveted lap joints are elevated significantly when they are changed to single-rivet joints.

Figure 17 shows the distribution of axial stress (normalized with respect to the applied nominal stress) at the upper-panel hole surface for infinitely wide multiriveted lap joints. The axial stress is plotted as a function of angle (from −90 to 90 deg) and depth ($t = 0.0$, 0.765, and 1.53 mm). The sealant changes the stress distribution at various depths and angles in both models. The peak tensile stress is lower, whereas the peak compressive stress is higher, when a sealant is used. The peak tensile stress is observed at angle 5 deg and 1.53-mm depth (the location of elements E and F). From the peak tensile stress point to 90 deg, the tensile stress decreases gradually and becomes zero between angles 30 and 40 deg; it then increases to the peak compressive stress at 90 deg. At the top surface of both models (depth 0 mm), from angle 0 to 90 deg, the stress increases to tensile when a sealant is used.

Figure 18 shows the curvature lines on the upper panel of the multiriveted lap joints with and without sealant. It can be seen that there is bending in the upper panel from point a to the vicinity of the rivet hole (point b). A small amount of bending takes place from the vicinity of point c to point d. When a sealant is used, the bending angle slightly decreases in the vicinity of the rivet hole (point b), and insignificant bending still occurs from the vicinity of point c to point d.

The peak stresses in the rivet elements are shown in Table 5. In the rivet shank the compressive stresses increase about 20 and 10% for standard riveted and countersunk joints, respectively. The shear stresses increase about 15 and 7% for the standard and countersunk cases, respectively. On the other hand, the axial tensile stresses are reduced significantly, about 33 and 52% for standard and countersunk, respectively. The axial compressive stresses are also reduced

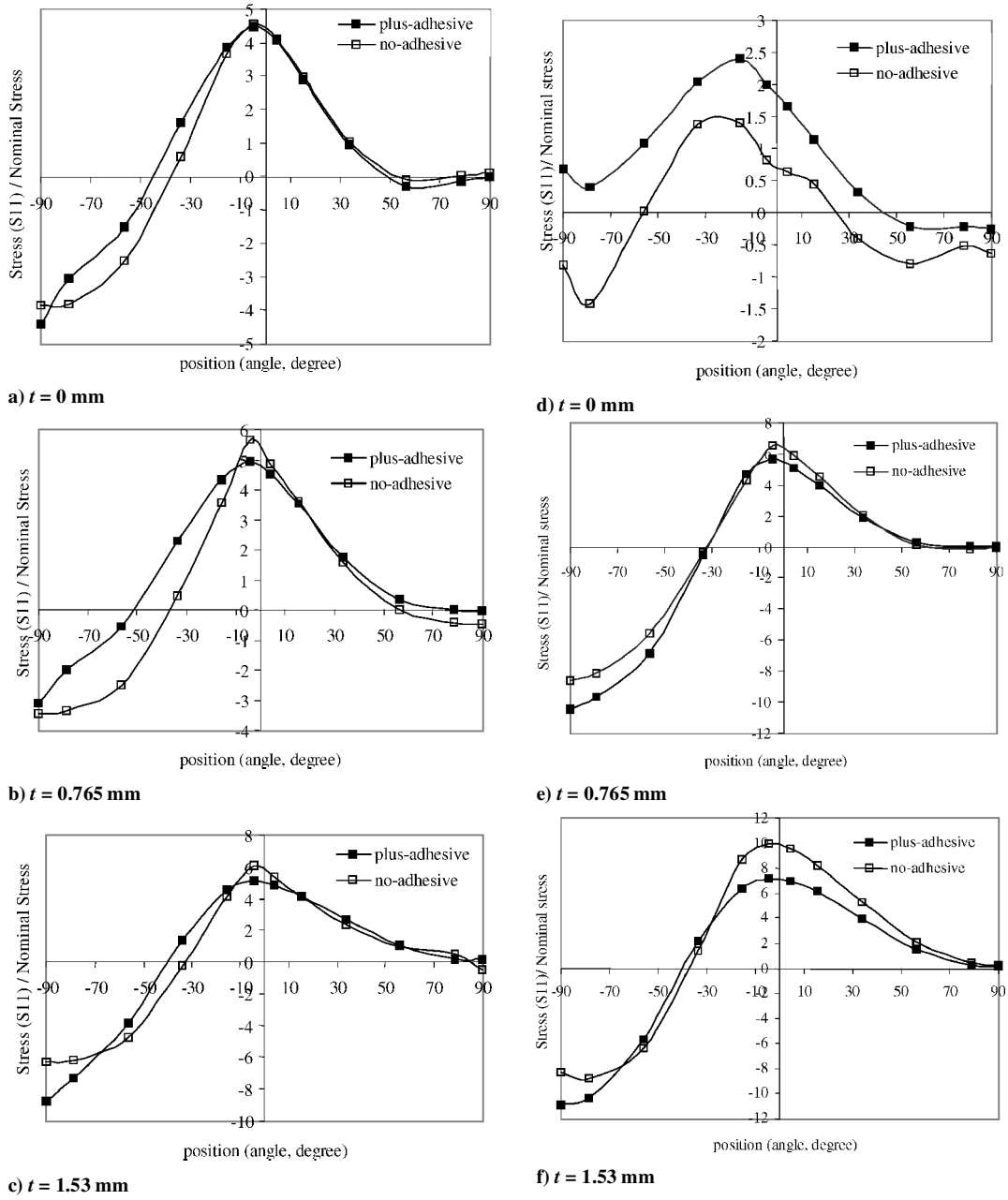

Fig. 17 Angular variation of normal stress (S11) around the surface of upper-panel hole for infinitely wide multiriveted lap joints: a), b), and c) are for models A-1-m and A-0-m and (standard single rivet-row plus-adhesive and no-adhesive, respectively) at depth 0, 0.765, and 1.53, respectively; d), e), and f) are for models B-1-m and B-0-m (countersunk single rivet-row plus-adhesive and no-adhesive) at depth 0, 0.765, and 1.53, respectively.

significantly (about 24% and about 44% for standard and countersunk, respectively).

Discussion

The TALA method is validated by comparisons with analytical solutions by Cornell[9] and Baker and Hatt[13] and by measurements of adhesive, adhesive-stepped, and sealed riveted lap joints. The results are in excellent agreement with the Baker and Hatt analysis because they treat a very thin layer of adhesive. The fact that Cornell treats a thick, rather than a thin, layer of brazing and includes the fillet effect at the brazed tab probably accounts for any discrepancies from the Cornell analysis. Small discrepancies in the experimental measurements are probably connected with the stress relaxation during displacement readings as well as uncertainties in the thickness of the sealant layers.

TALA has a number of unique and special features; it uses joint spring elements to simulate the actual adhesive material in two- and three-dimensional finite element models. It serves to reduce the required CPU time for the analyses. TALA is sensitive to the area and the thickness of the sealant volume. In addition, TALA is not limited to use only for bonding or sealing in riveted lap joints; it also can be used in other applications such as welding, gaskets, glazing, rubber sealing, or machine and bridge supports.

TALA can be used to study the effect of sealant on the mechanical behavior of riveted lap joints. It is shown here that the sealant influences the behavior in two major ways. First, a thin sealant layer at the interfacing surfaces acts like a lubricant, reducing the frictional resistance between the contacting surfaces and permitting large increases in the in-plane and out-of-plane slip. Iyer[25] showed that the in-plane and out-of-plane slip increases when the friction coefficient at all interfacing surfaces decreases. The decrease of dry friction obtained by Iyer[25] is consistent with the effect of sealant on slip obtained here. The reduced resistance to slip can also account for the increase in excess compliance and shank-hole contact pressure. Second, there is a large decrease in the out-of-plane separation

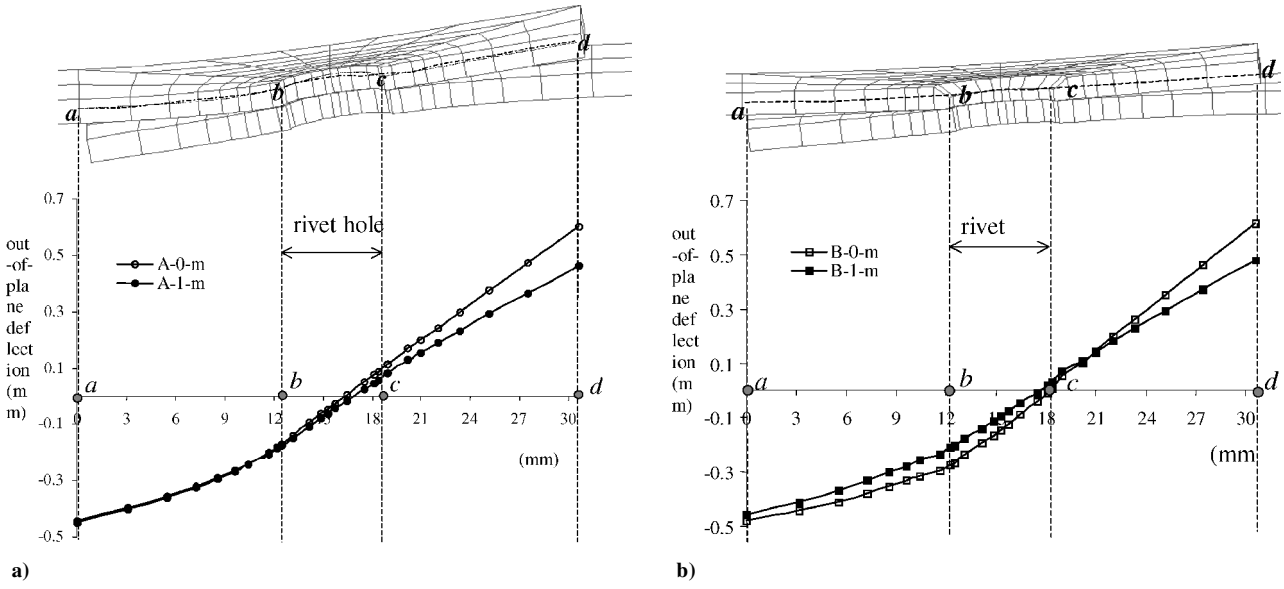

Fig. 18 Plots of the curvature line on the upper panel of infinitely wide multiriveted lap-joints models A-0-m and B-0-m (standard and countersunk single rivet-row, no-adhesive) and A-1-m and B-1-m (standard and countersunk single rivet-row, plus-adhesive).

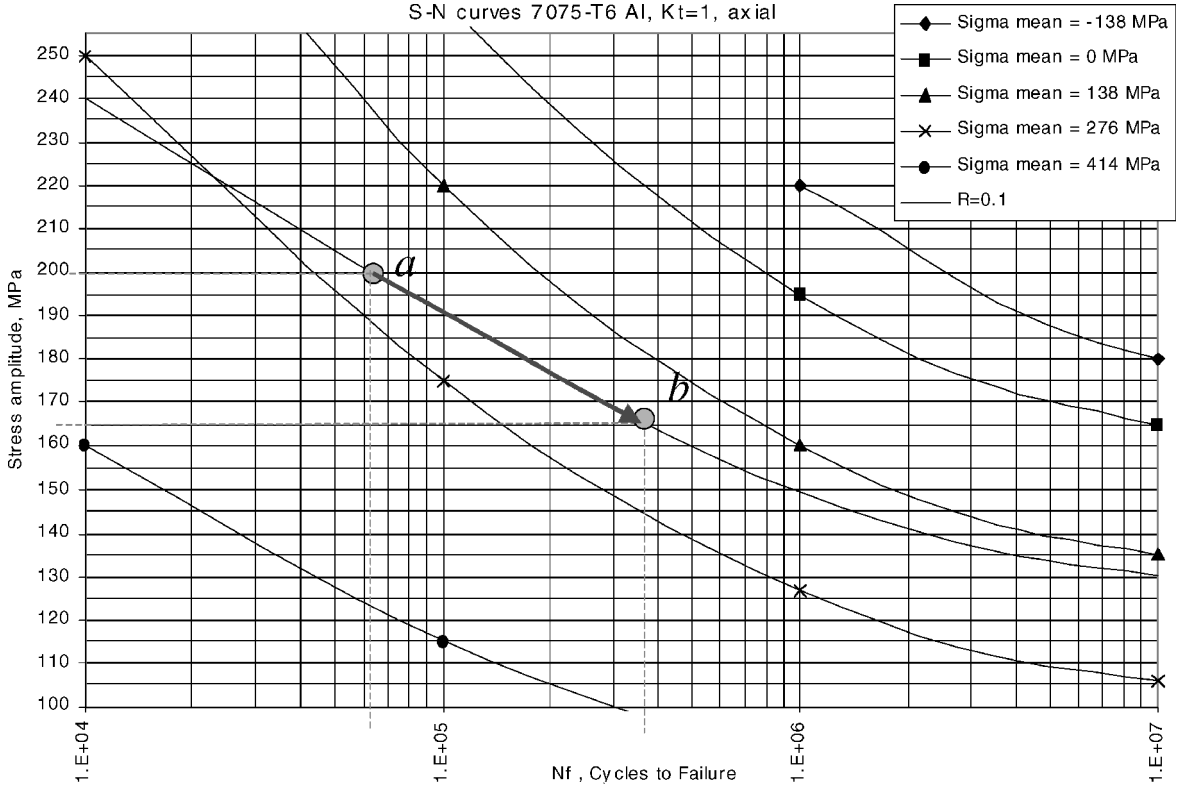

Fig. 19 Prediction of fatigue life using S-N curves for unnotched sample.

of the overlapping panels and a corresponding, but small, decrease in the panel curvature near the rivet hole. This is undoubtedly caused by the adhesive properties of the sealant. The shear moment acting on the rivet shank causes rivet tilt. This tilting induces the ends of the panels to bend in opposite directions and causes the panels to separate. The tensile stiffness of the sealant resists separation and reduces panel bending, local curvature, and rivet tilt. By reducing the bending, the sealant reduces the bending stresses that add to the in-plane stress, thereby reducing the SCF in the panels. The reduced bending also relieves the panel–panel pressure.

It is probable, based on the results presented here, that stiffer, higher-modulus adhesives, such as epoxies, will decrease panel bending, peak tensile stress, and slip in the joints, producing further reductions in SCF. This benefit is limited to the panel–panel separation and is small relative to other distortions. Decreasing adhesive layer thickness increases the stiffness of the adhesive layer; this would decrease the compliance, the panel bending, and the SCF in the same way.

Figure 19 presents estimates of how the fatigue life increases when the SCF decreases. For standard riveted lap joints the peak amplitude stress in the panel is reduced from 200 to 166 MPa (corresponding to a 17% reduction in SCF) at $R = 0.1$ when sealant is used. This fatigue life would be expected to increase from 60,000 to 350,000 cycles (about 483%). For countersunk riveted lap joints the peak stress amplitude in the panel is reduced from 200 to 144 MPa (corresponding to a 28% reduction in SCF) at $R = 0.1$ when the

sealant is used. Accordingly, the fatigue life would be expected to increase from 60,000 to 1,000,000 cycles (about 2400%).

Conclusions

1) A thin adhesive layer analysis (TALA) has been devised for use with the finite element program ABAQUS to evaluate the mechanical effects of thin layers of sealant or adhesive on riveted lap joints. The analysis represents the adhesive with spring elements whose stiffness is derived from measurements of the nonlinear, adhesive tensile, and pressure-dependent shear compliances.

2) TALA has been validated by comparisons with previous analyses of the pure bending and pure shear of brazed and adhesive lap joints, respectively. In addition, TALA calculations of the in-plane and out-of-plane load-displacement curves of adhesive, adhesive stepped and riveted plus adhesive lap joints agree closely with measurements.

3) TALA has been used to evaluate the effect of a sealant on the local stresses and the distortions of finite width single-rivet and infinitely wide multiriveted lap joints. The sealant produces a large decrease in the out-of-plane separation of the overlapping panels and a corresponding, but smaller, decrease in the panel curvature near the rivet hole and in the rivet tilt. By reducing the bending, the sealant reduces the bending stresses, which add to the in-plane stress, thereby reducing the stress concentration factor (SCF) by about 17 and 28% for standard and countersunk riveted lap joints, respectively. The reduced bending also relieves panel-panel contact pressure.

4) The finite element calculations reveal that the sealant produces large increases in the in-plane and out-of-plane slip at the rivet–panel interfaces and a smaller increase in the excess compliance. It also increases the shank–hole contact pressure.

5) The finite element calculations reveal that the sealant increases the shear stress and compressive stress at the rivet shank in the in-plane direction; on the other hand, it decreases the axial tensile stress in the out-of-plane direction.

6) The reduction in SCF produced by the sealant is expected to be accompanied by a 483 to 2400% increase in the fatigue life of the riveted lap joints.

Acknowledgments

The authors are grateful to Hibbitt, Karlsson, and Sorensen, Inc., for permission to use the finite element code ABAQUS. Computations were performed on the SGI Power Challenge Array at the National Center for Supercomputing Applications, Illinois. The authors also thank Notsanop Kamnerdtong, Thongchai Fongsamootr, and Pedro Bastias for their advice and support; Paul Nelson from Textron Aerostructures in Nashville, Tennessee, who helped with sample preparation; and Bill Keller from PRC-DeSoto International, Inc. (formerly Courtalds Aerospace), who provided the test sealants.

References

[1]Volkerson, O., "Die Nietkraftverteilung in Zugbeanspruchten Nietverbindungen mit Konstanten Laschenquerschnitten," *Luftfahrtforschung*, Vol. 15, 1938, pp. 41-47.

[2]Goland, M., and Reissner, E., "The Stresses in Cemented Joints," *Journal of Applied Mechanics*, Vol. 11, 1944, pp. A17–A27.

[3]Hart-Smith, L. J., "Adhesive Bonded Single Lap Joint," NASA CR-112236, Jan. 1973.

[4]Chen, D., and Cheng, S., "An Analysis of Adhesive Bonded Single Lap Joint," *Journal of Applied Mechanics*, Vol. 50, 1983, pp. 109–115.

[5]Ojalvo, I. U., and Eidinoff, H. L., "Bonded Thickness Effects upon Stress in Single Lap Joints," *AIAA Journal*, Vol. 16, 1978, pp. 204–211.

[6]Oplinger, D. W., "Effect of Adherend Deflections in Single Lap Joints," *International Journal of Solids and Structures*, Vol. 31, 1994, pp. 2565–2587.

[7]Tsai, M. Y., and Morton, J., "An Evaluation of Analytical and Numerical Solutions to Single Lap Joint," *International Journal of Solids and Structures*, Vol. 31, 1994, pp. 2537–2563.

[8]Tsai, M. Y., Oplinger, D. W., and Morton, J., "Improved Theoretical Solutions for Adhesive Lap Joints," *International Journal of Solids Structures*, Vol. 35, 1998, pp. 1163–1185.

[9]Cornell, R. W., "Determination of Stresses in Cemented Lap Joints," *Journal of Applied Mechanics*, Vol. 75, 1953, pp. 355–364.

[10]Wooley, G. R., and Carver, D. R., "Stress Concentration Factors for Bonded Lap Joints," *Journal of Aircraft*, Vol. 8, 1971, pp. 817–820.

[11]Adam, R. D., and Pepiatt, N. A., "Stress Analysis of Adhesively Bonded Lap Joints," *Journal of Strain Analysis*, Vol. 9, 1974, pp. 185–196.

[12]Crocombe, A. D., and Adams, R. D., "Influence of the Spew Fillet and others Parameters on the Stress Distribution in the Single Lap Joint," *Journal of Adhesion*, Vol. 13, 1981, pp. 141–155.

[13]Baker, M. R., and Hatt, F., "Analysis of Bonded Joints in Vehicular Structures," *AIAA Journal*, Vol. 11, No. 12, 1973, pp. 1650–1654.

[14]Prickett, A. K., and Holloway, L., "The Analysis of Elastic–Plastic Adhesive Stress in Bonded Lap Joints in FRP Structures," *Composite Structure*, Vol. 4, 1985, pp. 135–160.

[15]Harris, J. A., and Adams, R. D., "Strength Prediction of Bonded Single Lap Joints by Nonlinear Finite Element Methods," *International Journal of Adhesion and Adhesives*, Vol. 4, 1984, pp. 65–78.

[16]Crocombe, A. D., and Bigwood, D. A., "Development of a Full Elasto–Plastic Adhesive Joint Design Analysis," *Journal of Strain Analysis*, Vol. 27, 1992, pp. 211–218.

[17]Reddy, J. N., and Roy, S., *Finite-Element Analysis of Adhesive Joints*, Plenum, New York, 1991, pp. 359–394.

[18]Nagaraja, Y. R., and Alwar, R. S., "Viscoelastic Analysis of an Adhesive-Bonded Plane Lap Joint," *Computers and Structures*, Vol. 6, 1980, pp. 621–627.

[19]Pandey, P. C., Shankaragouda, H., and Singh, A. K., "Nonlinear Analysis of Adhesively Bonded Lap Joints Considering Viscoplasticity in Adhesives," *Computers and Structures*, Vol. 70, 1999, pp. 387–413.

[20]Pascal, J., Darque-Ceretti, E., Felder, E., and Pouchelon, A., "Rubber-Like Adhesive in Simple Shear: Stress Analysis and Fracture Morphology of a Single Lap Joint," *Journal of Adhesion Science and Technology*, Vol. 8, 1994, pp. 553–573.

[21]Ekvall, J. C., "Fatigue of Riveted Metallic Joints," *ASTM Special Technical Publication*, Vol. 927, 1986, pp. 172–189.

[22]Weissberg, V., Wander, K., and Itzhakov, R., "A New Approach to Load Transfer in Bolted Joints," *16th Congress of the International Council of Aeronautical Sciences*, Vol. 1, AIAA, Washington, DC, 1988, pp. 96–101.

[23]Swenson, D. V., Gondhalekar, S. R., and Dawicke, D. S., "Analytical Developments in Support of the NASA Aging Aircraft Program with an Application to Crack Growth from Rivets," Society of Automotive Engineers, ISSN 0148-7191, 1993.

[24]Fung, P., and Smart, J., "An Experimental and Numerical Analysis of Riveted Single Lap Joints," *Proceedings of the Institution of Mechanical Engineers, Part G, Journal of Aerospace Engineering*, Vol. 208, 1994, pp. 79–90.

[25]Iyer, K., "Three-Dimensional Finite Element Analyses of the Local Mechanical Behavior of Riveted Lap Joints," Ph.D. Dissertation, Dept. of Mechanical Engineering, Vanderbilt Univ., Nashville, TN, May 1997.

[26]Imanaka, M., "Fatigue Strength of Adhesive/Rivet Combined Lap Joints," *Journal of Adhesion*, Vol. 49, 1995, pp. 197–209.

[27]Liu, J., and Sawa, T., "Stress Analysis and Strength Evaluation of Single-Lap Adhesive Joints Combining Rivets Subjected to External Bending Moments," *ASME Proceedings, Reliability, Stress Analysis, and Failure Prevention Issues in Adhesive and Bolted Connections*, DE-Vol. 105, edited by E. Sancaktar, American Society of Mechanical Engineers, New York, 1999.

[28]Kamnerdtong, N., "Characterization of the Behavior of Thin Polymer Layers for Use in the Analysis of Riveted Connections," M.S. Thesis, Dept. of Mechanical Engineering, Vanderbilt Univ., Nashville, TN, May 1998.

[29]Fongsamootr, T., "Characterization of Thin Polymer Layer as a Frictional Interface for Use in the Analysis of Riveted Connections," M.S. Thesis, Dept. of Mechanical Engineering, Vanderbilt Univ., Nashville, TN, May 1998.

[30]Fongsamootr, T., "The Dilation and Compressive Properties of a Polymer Sealant and Analyses of the Distortion and Fatigue of Sealed Riveted Lap Joints," Ph.D. Dissertation, Dept. of Mechanical Engineering, Vanderbilt Univ., Nashville, TN, Dec. 2001.

[31]Kamnerdtong, N., "The Shear Properties of a Polymer Sealant and Analyses of the Distortion and Fatigue of Sealed Countersunk Riveted Lap Joints," Ph.D. Dissertation, Dept. of Mechanical Engineering, Vanderbilt Univ., Nashville, TN, Dec. 2001.

[32]Dechwayukul, C., "Development of a Thin Adhesive Layer Analysis for Riveted and Other Structural Joints," Ph.D. Dissertation, Dept. of Mechanical Engineering, Vanderbilt Univ., Nashville, TN, Dec. 2001.

[33]"ABAQUS Users Manual," Ver. 5.8.2, Hibbit, Karlsson and Sorensen, Inc., Pawtucket, RI, 2000.

[34]Al-Dakkan, K., "The Effect of Interference on Fatigue Life in Single-Rivet Row Aluminum Lap Joints," M.S. Thesis, Dept. of Mechanical Engineering, Vanderbilt Univ., Nashville, TN, Aug. 2000.

[35]Huang, Y., "The Effect of Interference on Fatigue Life in Single and Double-Rivet Row Aluminum Lap Joints," M.S. Thesis, Dept. of Mechanical Engineering, Vanderbilt Univ., Nashville, TN, Dec. 2000.

S. Saigal
Associate Editor